Feedback-Controlled MEMS Force Sensor for Characterization of Microcantilevers

Steven Ian Moore, M. Bulut Coskun, Tuncay Alan, Adrian Neild, and S. O. R. Moheimani, *Fellow, IEEE*

***Abstract*— This paper outlines the design and characterization of a setup used to measure the stiffness of microcantilevers and other small mechanical devices. Due to the simplicity of fabrication, microcantilevers are used as the basis for a variety of mechanical sensor designs. In a range of applications, knowledge of the stiffness of microcantilevers is essential for the accurate calibration of the sensors in which they are used. Stiffness is most commonly identified through measurement of the microcantilever's resonance frequency, which is applied to an empirically derived model. This paper uses a microelectromechanical system (MEMS)-based force sensor to measure the forces produced by a microcantilever when deformed and a piezoelectric tube-based nanopositioner to displace the microcantilever. A method of calibrating the force sensor is presented that takes advantage of the lumped nature of the mechanical system and the nonlinearity of MEMS electrostatic drives. [2014-0183]**

***Index Terms*— Microelectromechanical systems, nanopositioning, microcantilevers, displacement measurement, force measurement, stiffness identification.**

I. Introduction

THE DEVELOPMENT of microelectromechanical systems (MEMS) has seen mechanical phenomena used as the basis for a wide range of sensing technologies [1], [2]. MEMS are miniature mechatronic systems produced using microfabrication techniques [3]. One of the simplest and most common MEMS structures in use is the microcantilever [4]–[6].

In response to some input stimulus, changes in the properties or states of a microcantilever occur which can be electronically sensed. Typically, it is the static deflection or resonant frequency of the microcantilever that is of interest [7]. Piezoelectric transducers, piezoresistive transducers or optical detectors are common technologies used to monitor the motion of the microcantilever.

This work presents a setup to measure the stiffness of microcantilevers. In cases where microcantilevers are used for force measurement, the stiffness of the microcantilever is an important parameter to identify. An example of an area where the calibration of microcantilevers is of benefit is force microscopy [8], where the measurement of forces in micro and nanoscale systems has become of increasing interest [9], [10]. While this setup is demonstrated on microcantilevers, the identification of stiffness has applications with other microscale mechanical structures. For example stiffness measurements could be used to determine the mechanical integrity of MEMS devices [11] and there are a number of applications in the biomedical field [9], [10], [12], [13]. In particular, cancer cells have been shown to be significantly softer than the surrounding tissue [9].

Numerous approaches have been develop to measure the stiffness of microcantilevers. Sader's method [14] uses the identified resonance frequency and maps this to stiffness using material density and microcantilever dimensions. The thermal tune method [15] identifies a number of microcantilever parameters by analyzing the power spectral density at the output of the displacement sensor while only thermal noise is exciting the microcantilever. Many authors [11], [16], [17] use a reference microcantilever whose stiffness is known to identify the stiffness of an unknown microcantilever. Grutzik *et al.* [18] provides a methodology that follows a set of steps: calibration of a load cell using known weights, calibration of an indenter using the load cell and then the use of the indenter to characterize the microcantilever. Miyamoto *et al.* [19] modified a macro sized load cell to achieve force and displacement resolutions suitable for micro-system testing.

In this work, a MEMS device is used to measure the force imparted by the deflected microcantilever. The basic principle used in many MEMS force sensors is to measure the displacement of a mechanical structure and relate it to force with an identified stiffness [17], [20]–[24]. Of issue with this principle is the uncertainty in the stiffness identification and the change in stiffness with large deflections. This work utilizes feedback to keep the mechanical structure in its null position [25]–[30] which avoids the nonlinearity and makes the sensitivity of the force a function of actuator parameters.

This paper outlines a setup to measure the stiffness of microcantilevers. It utilizes direct measurements of force generated by a microcantilever as it is deflected. Due to the small size of the sample, two nanopositioning devices are used to perform these measurements. A MEMS nanopositioner in conjunction with feedback control is used to measure the force applied to its stage. By keeping the stage in its null position,

Manuscript received June 18, 2014; revised October 1, 2014; accepted November 2, 2014. Date of publication January 12, 2015; date of current version July 29, 2015. This work was supported by the Australian Research Council. Subject Editor O. Tabata.

S. I. Moore and S. O. R. Moheimani are with the School of Electrical Engineering and Computer Science, University of Newcastle, Callaghan, NSW 2308, Australia (e-mail: steven.i.moore@uon.edu.au; reza.moheimani@newcastle.edu.au).

M. B. Coskun, T. Alan, and A. Neild are with the Department of Mechanical and Aerospace Engineering, Monash University, Melbourne, VIC 3145, Australia (e-mail: bulut.coskun@monash.edu; tuncay.alan@monash.edu; adrian.neild@eng.monash.edu.au).

Color versions of one or more of the figures in this paper are available online at http://ieeexplore.ieee.org.

Digital Object Identifier 10.1109/JMEMS.2014.2382648

the action of the controller becomes proportional to the force applied. A piezoelectric tube nanopositioner is used to displace the microcantilever, and its displacement is sensed with a capacitive sensor. This technique is such that it can be applied to other structures to characterize its mechanical properties.

This work builds on the previous study by Coskun *et al.* [31]. This paper provides a complete description of the system and contains a number of refinements to the force sensor. The original device exhibited a quadratic nonlinearity in the force sensor sensitivity. In this paper, an analog front end is presented as an effective solution to linearize the sensor. The calibration method presented relies on direct measurements of the MEMS device displacement and capacitance. The original method was based on finite element analysis which requires precise measurements of the geometry of the manufactured device and is prone to errors if the fabrication process is not ideal, for example, if finger pairs are damaged or missing. Finally, the setup introduces a piezoelectric tube nanopositioner to ramp the sample into the force sensor which includes a capacitive sensor for accurate displacement measurement. A combination of its accurate real time displacement measurement and ramp characteristic make the method faster and more robust in the presence of noise and disturbances in comparison to the step responses used in [31].

Section II introduces the MEMS nanopositioner and describes its fabrication, actuation and sensing circuitry. Section III outlines the identification of the MEMS nanopositioner. Section IV provides the control design, analysis and implementation and presents the noise performance of the force sensor in operation. Section V will outline the methodology to combine the MEMS force sensor with a piezoelectric tube nanopositioner to make stiffness measurements of a microcantilever. Section VI outlines the experimental identification of one microcantilever using this methodology.

II. The Design of the MEMS Force Sensor

The MEMS nanopositioner to be used as a force sensor is shown in Figure 1. The device is fabricated in a 25 µm layer of single-crystal-silicon resting on a silicon oxide coated substrate. The substrate is etched through to release the device. The fabrication is performed using the SOIMUMPS fabrication process provided by MEMSCAP.

The device consists of a central stage whose motion is constrained to one-degree-of-freedom by a set of clamped-guided flexures on either side. This electromechanical system can be considered as a lumped mass-spring-damper system. There are two sources of input stimuli for this system. The first comes from an external force applied to a small flat tip on the edge of the stage. This is the force to be measured by this force sensor. The second is the actuation force generated by an electrostatic comb drive attached to the stage. The displacement of the stage is captured using an electrothermal position sensor. The schematic of the MEMS nanopositioner is shown in Figure 2.

An electrostatic comb drive [2] is comprised of two electrodes in close proximity to form a capacitive structure. Each electrode consists of an array of fingers that are interwoven with the other. One electrode is typically fixed while the other has its motion constrained to one-degree-of-freedom. For the comb drive used in this work, the motion of the drive is constrained such that the gap between the fingers is constant and the electrode overlap can change. When a voltage is applied across the electrodes an attractive force develops. Using the definition of force as the rate of change of energy with respect to displacement, the force as a function of voltage can be derived and it is shown in Equation (1) below.

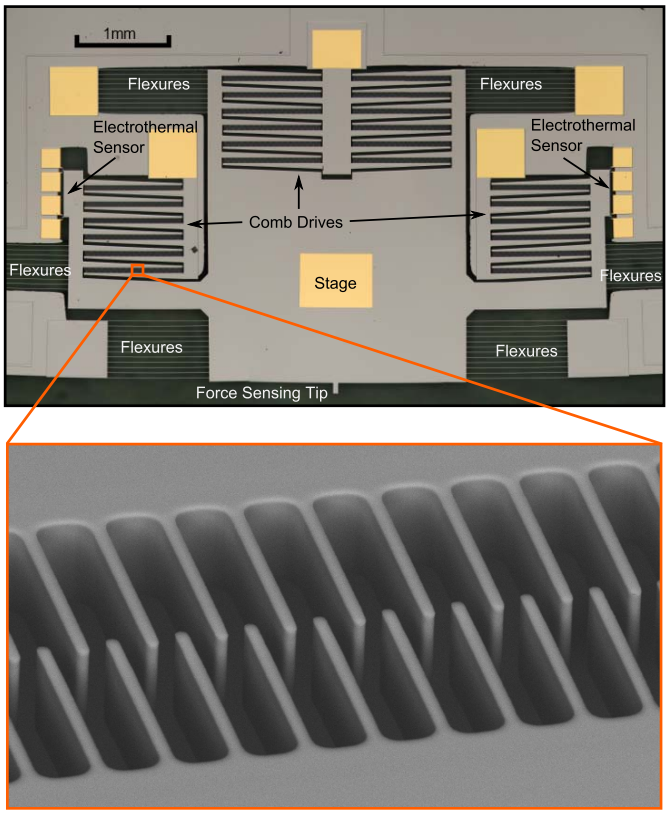

Fig. 1. An image of the MEMS nanopositioner. The device consists of a stage whose motion is constrained to one-degree-of-freedom with a set of clamped-guided flexures. A set of comb drives are used to actuate the nanopositioner. The force to be measured is applied to a flat tip on the edge of the stage. Electrothermal sensors to the side of the stage are used to measure displacement. The close up shows the structure of the comb drives. It consists of an array of interwoven fingers that make a capacitive structure. The length of each finger is 30 μm and the gap between them is 2 μm.

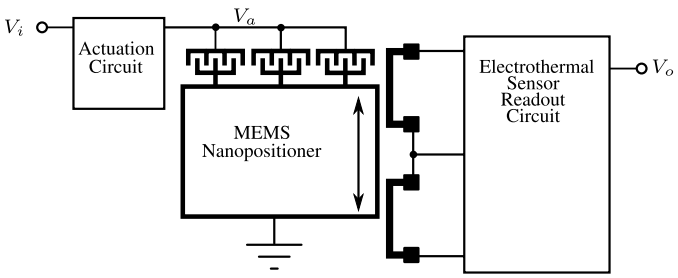

Fig. 2. The schematic of the MEMS nanopositioner. An actuation circuit applies a voltage across the three comb drives in parallel. The actuation circuit performs amplification and cancels the nonlinearity in the comb drives. The displacement is readout using an electrothermal sensor that consists of two resistive elements in a differential arrangement in close proximity to the nanopositioner's stage.

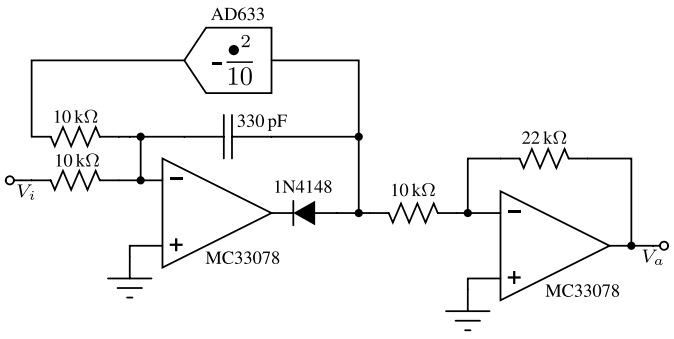

Fig. 3. The actuation circuit implements a square root function to compensate for the nonlinearity of the comb drive. The first op amp is configured as an integrator to reduce the bandwidth of the system to keep the circuit stable. The diode prevents the op amp from latching to a permanently unstable state when the input goes negative.

A parameter known as the comb drive constant, η, is defined to capture the combination of the constant terms in this equation [2].

$$f_e = \frac{n\varepsilon h}{2g} V_a^2 \tag{1}$$

$$= \eta V_a^2 \tag{2}$$

In this device the electrode height h is 25 μm, the electrode gap g is 2 μm, the number of overlapping faces n is 5832 and ε is the permittivity of free space. The comb drive constant η is 322.7 nN V^{-2}. Note that this value is determined based on a simplified model and serves to aid the design of the force sensor. A more accurate value is required to derive the sensitivity of the force sensor. This can be determined through finite element analysis factoring in the post-fabrication dimensions of the device and the effects of fringing fields as reported by Coskun *et al.* [31]. This, however, is potentially laborious. An experimental procedure to evaluate η is presented in Section III.

Nonlinearity is an important sensor characteristic to consider and the quadratic mapping from voltage to force of the comb drive is the main source of nonlinearity in this system. Removing this nonlinearity from a MEMS nanopositioning system by inverting its characteristic has been successfully demonstrated to linearize comb drives by Mohammadi *et al.* [32]. In this work, to compensate for the nonlinearity, the comb drive actuation circuit is instrumented with a square root characteristic. The circuit is shown in Figure 3. The low frequency mapping from the input voltage V_i to the actuation voltage V_a is given in Equation (3) below.

$$V_a = 2.2\sqrt{10 V_i} \tag{3}$$

Equation (1) and Equation (3) are combined and the result is shown in Equation (4) below. It shows that the ideal system is linear. The gain from the input voltage V_i to the comb drive force f_e is 15.62 μN V^{-1}.

$$f_e = 48.4\eta V_i \tag{4}$$

$$= 15.62 \times 10^{-6} V_i \tag{5}$$

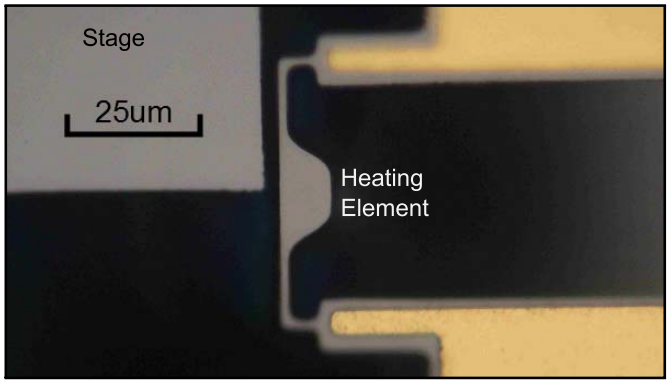

Fig. 4. A photo of a resistive element in an electrothermal sensor used to measure the displacement of the MEMS nanopositioner. When heated by a bias current, the temperature is a function of the displacement of the stage that can be seen in close proximity to it. The resistance of the element is a function of its temperature. The length of the resistive element shown is 50 μm.

The sensor's output is ideally proportional to the force and nonlinearity represents a deviation from this. This compensation has the benefit of allowing the force to be read out accurately without external compensation. The primary benefit of the compensation is that it makes the device linear for purposes of control. This allows for a powerful suite of techniques to analyze and design the force sensor's characteristics. In particular this makes the sensitivity and bandwidth constant over the entire range of the force sensor.

The preceding analysis assumes the parameter η is constant. This is based on the assumption that the electric field is uniformly distributed between the fingers. The fringing fields that exist in the electrostatic drive need to be considered for an accurate determination of η. There exists two potential effects. First is the case where η is still constant but is different from the ideal value due to the fringing fields. The finite element simulations in the work by Coskun *et al.* [31] or the measurements presented in this paper do not rely on any assumptions about the distribution of the electric field and would detect this discrepancy. The second effect is that the fringing fields make η vary with displacement. This would exhibit itself as a nonlinearity in the MEMS device. The proceeding results will show that the nonlinearity is insignificant in this device.

The electrothermal position sensor [33], [34] consists of a pair of resistive elements in close proximity to the stage. An image of a resistive element is shown in Figure 4. A bias voltage is placed across the resistive elements to raise their temperature. The temperature of each sensor is a function of the heat conduction between it and the stage. As the overlap between the stage and the resistive elements changes, the heat conduction, and thus the temperature of the resistive elements changes. Being made of doped silicon, this change of temperature leads to variations in the resistance of the elements. This change in resistance can be read out electrically.

The shape of the resistive elements is based on the work reported in Fowler *et al.* [34] in which the shape was designed to achieve an even temperature distribution across the resistive elements. When compared to the resistive elements with a uniform cross section, these shaped resistive elements

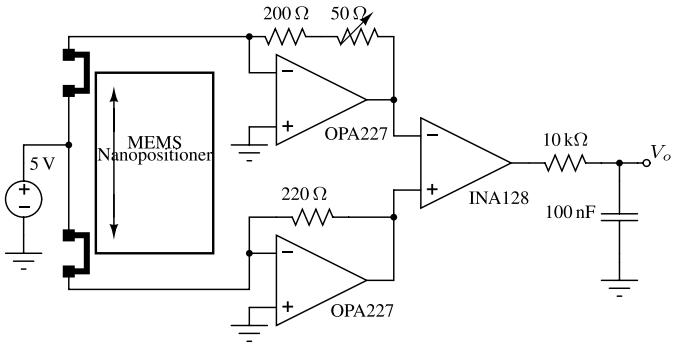

Fig. 5. The schematic of the electrothermal sensor readout circuit. To the left of the schematic is the MEMS device with two resistive elements whose resistance changes with displacement. A 5 V source is used to heat the resistive elements. The current though the resistors is measured with transimpedance amplifiers and the difference is taken using an instrumentation amplifier with a gain of 1065. Filtering is performed at the output. The op amps and instrumentation amplifier are from Texas Instruments.

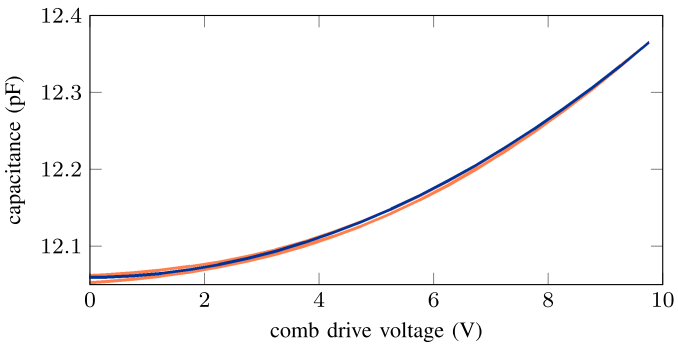

Fig. 6. The capacitance of the MEMS comb drive as a function of the comb drive voltage. This characteristic is measured using an LCR meter. The equation of the fitted blue curve is $C = 3.198 \times 10^{-3} V_a^2 + 12.06$ where capacitance is in pF. The discrepancy between the two traces is attributed to the imperfect decoupling between the LCR meter and the bias voltage source.

demonstrated a higher sensitivity, lower nonlinearity, lower noise floor and lower bandwidth.

The read out circuit is shown in Figure 5. The simplicity of the readout circuit is one of the main advantages of electrothermal displacement sensors. The resistance is measured by placing a constant voltage across the resistive elements and measuring the current through them using transimpedance amplifiers. As the resistive elements are arranged in a differential manner, an instrumentation amplifier is used to take the difference between them. The potentiometer shown in Figure 5 is used to zero the sensor. A low pass filter has been appended to the output of the electrothermal sensor to reduce the effect of the MEMS resonant motion on the force sensor design.

III. The Identification of the Force Sensor

Due to the way the force sensor will be operated, the comb drive constant η which maps the actuation voltage V_a to the comb drive force f_e is key to identifying the sensitivity of the force sensor. This parameter has been calculated from the design parameters. However, simplifications in the modeling and fabrication tolerances may lead to inaccuracies.

To identify η, the calibration method presented in this work is a new approach for a MEMS force sensors. The method is exploits the characteristics of the electrostatic drive that actuates the force sensor. This ultimately allows the calibration to be performed with a displacement and capacitive measurement, both of which are more simply and accurately preformed on microscale systems compared to producing an accurate calibrating force.

The idea to identify the comb drive constant η comes from the general expression for the force of a capacitive drive in Equation (6) below.

$$f_e = \frac{1}{2}\frac{\partial C}{\partial x} V_a^2 \tag{6}$$

$$= \eta V_a^2 \tag{7}$$

In Equation (6), the comb drive constant η is half $\partial C/\partial x$. If capacitance and displacement can be measured as a function of some intermediate variable, then the partial derivate can be found with the chain rule. In this work, voltage is the intermediate variable with $C(V)$ and $x(V)$ being measured directly.

The following calculations of η rely on the assumption that both η and device stiffness k are constant. When this is the case both the displacement x and the capacitance C will be quadratic functions of the actuation voltage squared V_a. Deviations from a quadratic characteristic would represent an error in the assumptions and would ultimately be observable as a nonlinearity in the sensor.

Therefore, to experimentally identify the parameter η, two static mappings are considered. The first is the mapping from the comb drive voltage V_a to the displacement x as shown in Equation (8) below.

$$kx = \eta V_a^2 \tag{8}$$

It is derived by equating the restoring force of the mechanical system, due to the stiffness k, with the force produced by the comb drive. The other is the mapping from displacement to capacitance as shown in Equation (9) below. The constant terms in the capacitance expression can be written in terms of η when Equation (8) is substituted in to remove displacement from the expression. C_p represents the parasitic capacitances in the system.

$$C = \frac{n\varepsilon h}{g} x + C_p \tag{9}$$

$$= \frac{2\eta^2}{k} V_a^2 + C_p \tag{10}$$

These two characteristics are measured to allow for the parameters η and k to be found. First, the comb drive of the MEMS positioner is connected to an LCR meter and the capacitance is measured. The result is shown in Figure 6. A quadratic fit was made and the resulting equation is $C = 3.198 \times 10^{-3} V^2 + 12.06$ where capacitance is in pF. Next the displacement was measured using a laser Doppler vibrometer while the device was actuated with a 1 Hz triangle wave. The result is shown in Figure 7. Another quadratic fit was made and the resulting equation is $x = 6.601 \times 10^{-3} V^2$ where displacement is in μm.

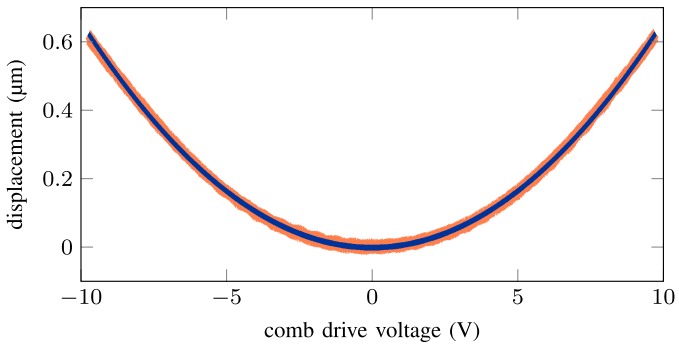

Fig. 7. The displacement of the MEMS device as a function of voltage. This characteristic is measured using a laser Doppler vibrometer. The equation of the fitted blue curve is $x = 6.601 \times 10^{-3} V_a^2$ where x is in μm.

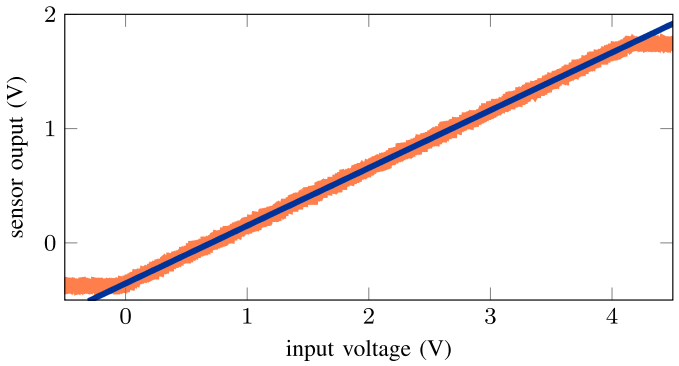

Fig. 8. The mapping from input voltage V_i to the output voltage V_o. The mapping is linear between the input voltage of 0 V and 4.1 V. A linear model was fitted (blue) to this mapping and it has a gain of 0.5044.

The coefficients of Equation (8) and Equation (9) are equated with the quadratic curves fitted to the measured results. Solving these equations, the comb drive constant η is $242.2\,\mathrm{nN\,V^{-2}}$ and the stiffness k is $36.7\,\mathrm{N\,m^{-1}}$. Considering the square root actuation circuit whose characteristic is described in Equation (3) in Section II, the experimentally identified gain from the input voltage V_i to the comb drive force f_e is $11.72\,\mu\mathrm{N\,V^{-1}}$.

When powered up, the MEMS device and associated circuitry consumed 1.74 W. Approximately 1 W is associated with the electrothermal sensor, its 5 V supply and the transimpedance amplifier feedback resistances. The rest is associated with the power consumption of the ICs. Next the static performance of the entire positioner was measured. The system was actuated from −0.5 V to 4.5 V and the sensor output was recorded. The result is shown in Figure 8. The nanopositioner has a low frequency gain of 0.5044. The input range of the nanopositioner was from 0 V to 4.1 V. The lower saturation limit is due to the diode in the square root circuit and the upper saturation limit is due to the saturation of the actuation circuit with a 15 V supply.

Considering the identified stiffness k, the identified comb drive constant η and the square root actuation circuit, the mapping from input voltage V_i to the displacement x has a gain of $0.3195\,\mu\mathrm{m\,V^{-1}}$. Therefore, when considering the gain of the entire MEMS system, the sensitivity of the electrothermal sensor is $1.579\,\mathrm{V\,\mu m^{-1}}$.

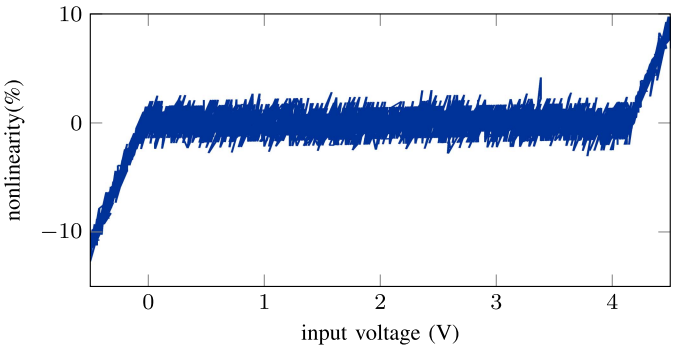

Fig. 9. The nonlinearity of the MEMS nanopositioner. It is defined as the difference between the measured data and the linear model expressed as a percentage of the full range. It shows there is no nonlinearity within the saturation limits. The small deviations around the linear fit are attributed to noise and disturbances.

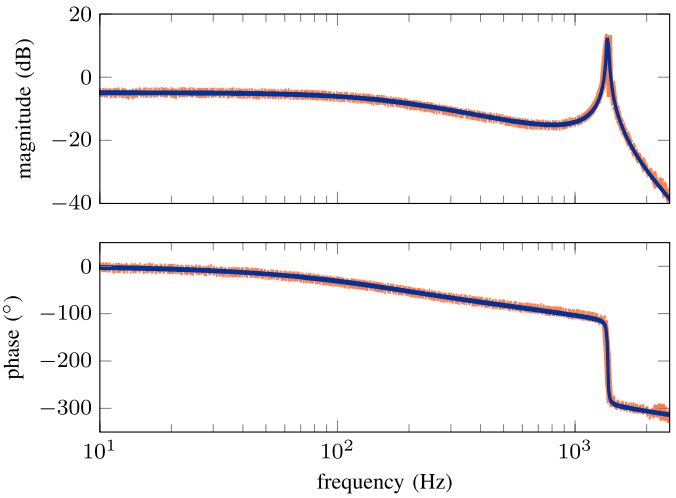

Fig. 10. The frequency response of the MEMS nanopositioner from input voltage to sensor output. The input voltage is biased at 1.5 V. The orange trace is the measured response using a sine sweep and the blue trace is a fitted linear model. A 4^{th} order model was found to provide a good fit.

The nonlinearity, defined as the difference between the measured and fitted characteristics as a percentage of full range, is shown in Figure 9. It can be observed that the actuation circuit successfully eliminates the quadratic characteristic of the comb drive from the system.

The entire system consists of a second order spring-mass-damper system in series with a first order electrothermal system. The electrothermal sensor readout circuit introduces one additional pole due to the filter at the output. The frequency response from the nanopositioner's input voltage to the displacement sensor output is shown in Figure 10. The expected dynamics are present with two lightly damped complex poles associated with the mechanical system and two real poles associated with the electrothermal sensor and circuit. A linear model is fitted and the transfer function is shown in Equation (11) below. The analysis of the control in the next section will be applied to this model.

$$G(s) = \frac{6.947 \times 10^{14}}{(s + 14820)(s + 1112)(s^2 + 98.01s + 7.398 \times 10^7)}. \tag{11}$$

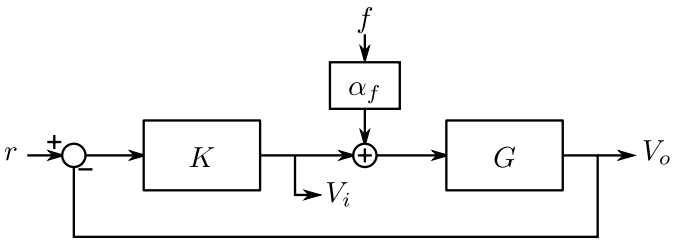

Fig. 11. [31] The topology of the control system. G is the MEMS device with a voltage input V_i and electrothermal sensor output V_o. The controller K is designed for disturbance rejection with the reference $r = 0$. As a sensor, the input disturbance f is the input stimulus and the value of the control action V_i is the output reading.

The dominant pole at $1112\,\mathrm{rad\,s^{-1}}$ is attributed to the filter at the output of the sensor. The other real pole is attributed to the electrothermal sensor system. The complex poles are attributed to the mechanical structure. The bandwidth of the system is 181.8 Hz.

IV. Control and Performance of the Force Sensor

The MEMS device is modeled as a second-order spring-mass-damper system as shown in Equation (12) below. An electrostatic force f_e is generated by the comb drives and an input force f, that is to be sensed, is applied to the device in the opposing direction.

$$m\ddot{x} + c\dot{x} + kx = f_e - f \tag{12}$$

A control system is designed to keep the stage in its null position. In steady state this implies $\ddot{x} = \dot{x} = x = 0$. Substituting this condition into Equation (12), the resulting equation relates the electrostatic force to the input force as shown in Equation (15). The electrostatic force is generated by a voltage placed across the comb drives. The comb drive constant η and the square root actuation circuit map the input voltage to the electrostatic force produced by comb drives. In the force sensor design, the force disturbance f is the input and MEMS input voltage V_i is the output. The parameter $\alpha_f = 1/(48.4\eta)$ is defined and it is the sensitivity of the force sensor. Using the identified value of η, the sensitivity of this force sensor is found to be $\alpha_f = 85.32\,\mathrm{kV\,N^{-1}}$.

$$f_e = f \tag{13}$$

$$48.4\eta V_i = f \tag{14}$$

$$V_i = \alpha_f f \tag{15}$$

The design specification for the control system is to keep the stage at its null position. With this specification and the transfer function G in Equation (11) in Section III, an integral controller seeks to keep the stage still. The transfer function of the controller is given in Equation (16). The integral controller has a gain of 555.6. Since the electrothermal sensors filter the resonant motion of the MEMS device, it is not critical to consider these dynamics in the design of the controller given the design specifications. Figure 11 contains a diagram of the control system. The complementary sensitivity function T of this closed loop system is shown in Figure 12. The complementary sensitivity function maps the reference r to the electrothermal sensor output V_o. It shows the controller

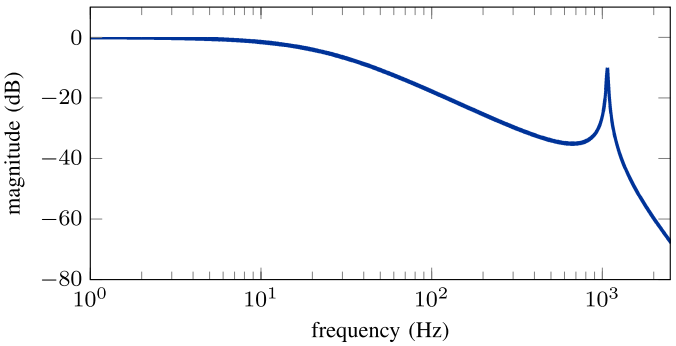

Fig. 12. The complementary sensitivity function T of the system. It is the mapping from the reference r to the electrothermal sensor output V_o. The control system has reference tracking up to a bandwidth of 68.75 Hz. Letting $r = 0$ will keep the stage still in response to low frequency disturbances.

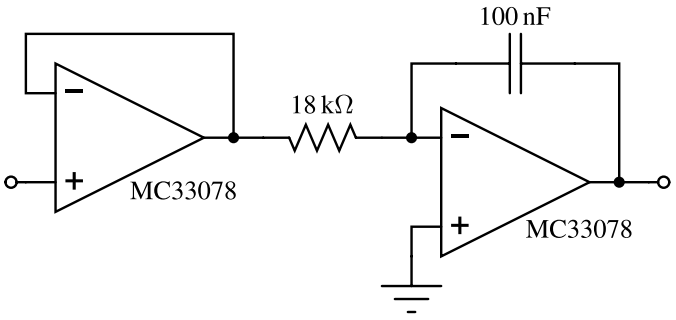

Fig. 13. The implementation of the integral controller to maintain the null position of the force sensor. The output of the electrothermal sensor is input directly into the controller as the setpoint $r = 0$ and the controller has an inverting characteristic.

will perform reference tracking up to 68.75 Hz. By letting $r = 0$ the controller will act to keep the stage in its null position.

$$K = \frac{555.6}{s} \tag{16}$$

The controller is implemented with an op amp circuit as shown in Figure 13.

With the control system in place the sensor operates as follows. The input stimulus to the sensor appears as an input disturbance. This is shown as the signal f in Figure 11. The controller will act to keep the stage still. Therefore, the control action V_i will compensate for the input disturbance. The control action becomes the output of the sensor. The transfer function S mapping the input disturbance to the control action is described as

$$S = \frac{V_i}{f} \tag{17}$$

$$= -\alpha_f T. \tag{18}$$

Here, T is the complementary sensitivity function whose magnitude response is shown in Figure 12. At low frequencies T has a gain of 1, thus the gain of S at low frequencies is α_f as expected. Additionally the sensor will have a bandwidth of 68.75 Hz. The range of the sensor is limited by the input voltage range of the MEMS nanopositioner which is from 0 V to 4.1 V. The voltage limit implies a force range of 48.05 μN.

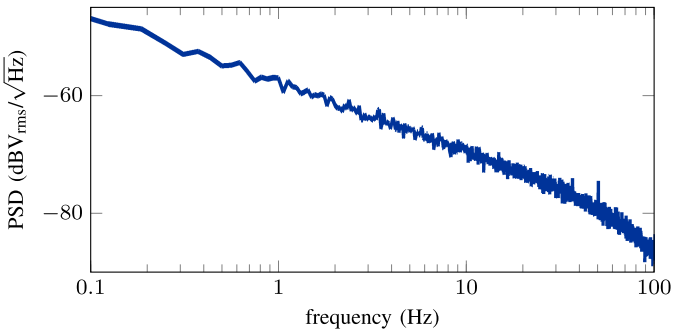

Fig. 14. The spectral density at the output of the force sensor. The resolution of the force sensor from 0.1 Hz to the sensor bandwidth of 68.75 Hz is 37.92 nN.

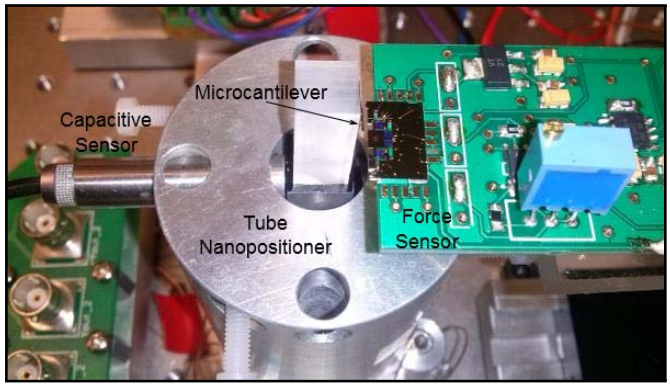

Fig. 15. Shown is the setup to measure the stiffness of a small sample. In this photo, the sample is a microcantilever that has been glued to a plastic piece fitted to a piezoelectric tube nanopositioner. The tube nanopositioner pushes the microcantilever against the force sensor. Its displacement is measured by a capacitive sensor.

The power spectral density at the output of the sensor is shown in Figure 14. Integrating the power spectral density from 0.1 Hz to the sensor bandwidth of 68.75 Hz, the 1σ resolution of the force sensor is 37.92 nN.

The nonlinearity of the sensor is inferred from the nonlinearity of the two systems it is composed of, that is the MEMS device and the controller. The MEMS device was shown to have minimal nonlinearity from the results shown in Figure 8 and Figure 9. With the sensor composed of this linear device and a linear controller in a feedback arrangement, the sensor is expected to also be linear.

V. Routine for Stiffness Characterization

To measure stiffness, a piezoelectric tube nanopositioner [35] is used to push a small sample against the MEMS force sensor. A capacitive sensor is used to measure the displacement of the tube nanopositioner. The stiffness, as the ratio of force over displacement, can be identified with the simultaneous capture of the force and displacement signals. A photo of the setup is shown in Figure 15 and a schematic of the setup is shown in Figure 16.

The tube nanopositioner consists of a solid piezoceramic tube with four electrodes on its outer surface spatially separated by 90°. The four electrodes share a common electrode

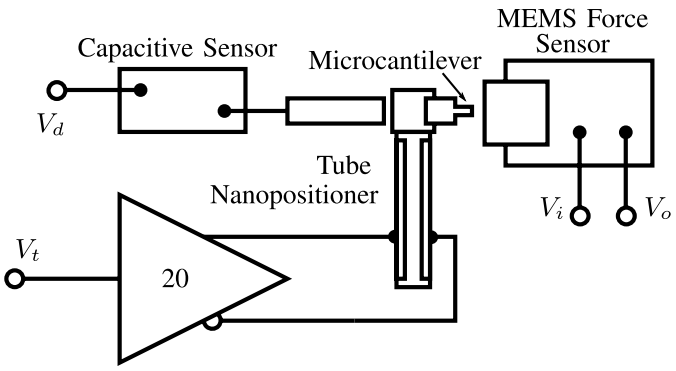

Fig. 16. This figure shows the schematic of the experimental setup used to measure the stiffness of a microcantilever. In the center is the tube nanopositioner upon which the microcantilever is mounted. To right is the MEMS device that is used as a force sensor. It is mounted on a manual positioner for coarse positioning. To the left is the capacitive sensor used to sense the motion of the tube nanopositioner. The entire setup is encased in a plastic box to isolate the exposed die from external air flows. An amplifier is used to drive the tube nanopositioner.

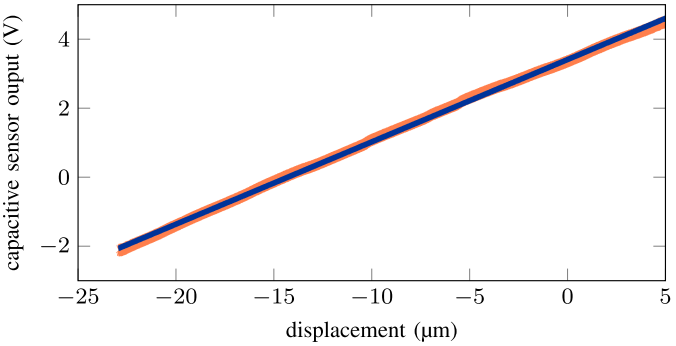

Fig. 17. Plotted is the output of the capacitive sensor on the tube nanopositioner as a function of the displacement along the x-axis as measured with a vibrometer. The fitted sensitivity (blue) of the capacitive sensor is 0.2384 MVm^{-1}.

on the inner surface of the tube. The inner electrode and the two y-axis electrodes are grounded. The two electrodes in the x-axis are excited with a differential voltage supplied by an amplifier with a gain of 20. To measure displacement, a capacitive sensor is placed in close proximity to a polished Aluminum block attached to the top of the tube. The capacitive sensor used is the model 8810 from Microsense.

It is important to identify the sensitivity of the capacitive sensor to achieve an accurate displacement measurement. In particular, the tube nanopositioner in this experiment was constructed at an angle to the table it is bolted to. This angle would introduce a scaling factor. The displacement is measured along the axis normal to the force sensor to identify the sensitivity of the capacitive sensor. This is performed with a laser Doppler vibrometer. The output of the capacitive sensor is plotted with respect to displacement in Figure 17. A linear model was fitted and the sensitivity of the capacitive sensor is determined as $\alpha_x = 0.2384\,\mathrm{MV\,m^{-1}}$.

To perform the stiffness measurement, first, the force sensor is brought into close proximity with the sample mounted to the tube nanopositioner. This is performed with a manual positioner. A microscope is used to assist with the alignment

of the sample. Once in place, a constant signal is applied to the tube nanopositioner to push the sample into contact with the force sensor. Then, a low frequency triangle wave is used to drive the tube nanopositioner. This drives the sample back and forth into the force sensor. The output of the MEMS force sensor and the output of the displacement sensor on the tube nanopositioner are captured with an oscilloscope.

Post processing is performed to extract the stiffness of the cantilever. First, the force data is expressed as a function of the displacement data. Assuming all the components in the system are linear, this function will be linear with gradient m_k. The stiffness of the microcantilever k_{mc} can then be expressed as a function of the gradient m_k, the sensitivity of the force sensor α_f and the sensitivity of the displacement sensor α_x. This expression is shown in Equation (19) below.

$$k_{mc} = m_k \frac{\alpha_x}{\alpha_f} \tag{19}$$

The setup used by Coskun et al. [31] uses a stepper motor to drive the microcantilever into the force sensor. In comparison, the tube nanopositioner provides a number of benefits to the experimental setup. It introduces a capacitive sensor to accurately capture the microcantilever's displacement which can be captured simultaneously with the force measurement. The ability to ramp the nanopositioner increases the speed of measurements for the stiffness identification. Combining both these features, the setup can capture a large number of data points in a short time. This minimizes the effect of noise and disturbances on the stiffness identification.

VI. The Experiment on a Microcantilever

The microcantilever upon which the experiment is performed is the model NSG01 from NT-MDT. The microcantilever is 130 µm long and 35 µm wide. It is made of silicon and its stiffness is specified to be within the range of $2.5\,\mathrm{N\,m^{-1}}$ to $10\,\mathrm{N\,m^{-1}}$. The microcantilever is mounted onto the tube nanopositioner, the force sensor is brought into close proximity to it, the tube nanopositioner is biased to push the microcantilever into contact with the force sensor and then the tube nanopositioner is driven with a 1 Hz triangle wave.

With the tube nanopositioner oscillating back and forth and the force sensor operating within its range, four signals are captured with an oscilloscope. These signals are the force sensor output (the MEMS device input voltage) V_i, the output of the capacitive sensor measuring displacement V_d, the waveform actuating the tube nanopositioner V_t and the output of the electrothermal sensors V_o. A capture of the signals is shown in Figure 18.

Firstly, it can be seen that the force sensor controller is operating correctly. The electrothermal sensor output is kept near zero, but has a slight offset. This is the characteristic of an integral controller in response to a ramp signal. The force and displacement measurements appear to follow the characteristic of the tube actuation voltage suggesting this experiment is operating in a linear region.

The force signal is plotted as a function of the displacement signal as shown in Figure 19. The stiffness of the microcantilever is assumed constant over the operating range

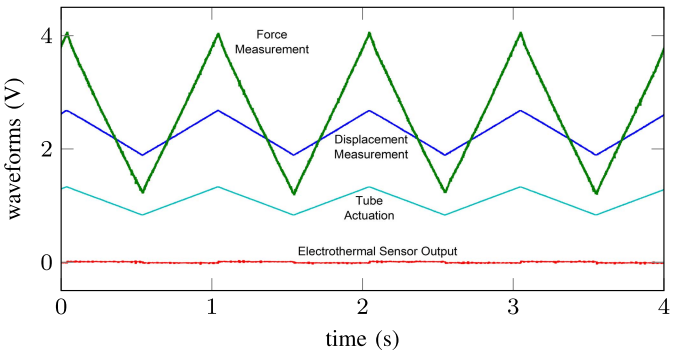

Fig. 18. A capture of the system's signals as the tube actuator is excited with a 1 Hz triangle wave. Shown is the force sensor measurement V_i, the displacement measurement using the capacitive sensor V_d, the tube nanopositioner actuation voltage V_t and the electrothermal sensor output V_o.

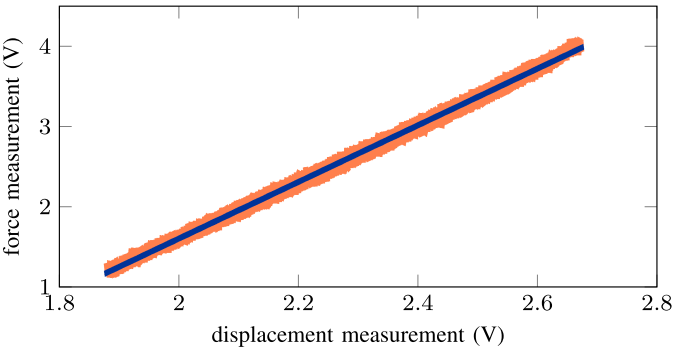

Fig. 19. Shown is the characteristic when the output of the force sensor is plotted with respect to the displacement sensor output. This uses the signals plotted in Figure 18. A linear model (blue) provides a good fit to the data, and the gradient of this model will be proportional to stiffness of the microcantilever. The gradient of the linear fit is 3.522.

of this experiment and thus a linear fit was made to this plot. The gradient of the fit is 3.522. Using the mapping between gradient and stiffness as outlined in Equation (19) in Section V, the stiffness of this cantilever is identified as $9.84\,\mathrm{N\,m^{-1}}$.

VII. Conclusion

Presented is a system for performing stiffness measurements on microscale systems. By utilizing nanopositioning technology, forces and displacements in microscale systems can clearly be captured.

The force sensor presented in this work is implemented with MEMS technology. MEMS allows for the freedom to implement more sophisticated mechanical designs. With the appropriate lumped mechanical design and the application of feedback control to keep the stage of the sensor in its null position, the sensitivity of the force sensor becomes solely dependent on the strength of the MEMS electrostatic actuator. This allows for identification of the sensitivity of the force sensor using capacitive and displacement measurements.

The accuracy of the stiffness measurement in this work is dependent on the accuracy of the calibration of the force sensor and the displacement sensor used with the tube nanopositioner. The calibrations provide the primary area for

improvement to the stiffness measurement performed in this article. Particularly for the force sensor, higher quality and more stringent measurement techniques would improve the accuracy of the displacement and capacitance measurements that are made in this article for calibration. Improvements to the measurement techniques could involve, for example, improved alignment of the vibrometer and better decoupling of the LCR meter from the bias voltage source. With greater attention paid to these measurements, the accuracy of the calibration could be quantified. With a more precisely calibrated force sensor, bounds on the force measurements could be specified and this would allow for a better determination of the uncertainty in the stiffness measurement.

Furthermore, the LCR meter and vibrometer that were used to perform these measurements may not be available in all cases. Though many other techniques exist to measure these quantities, an avenue to improve the device is the development of simpler or more accurate calibration methods that can be embedded into the circuitry or control of the force sensor.

With the demonstration of its suitability to measure stiffness demonstrated on microcantilevers, this system can easily be applied to measure the stiffness of other microscale systems.

REFERENCES

[1] J. Bryzek *et al.*, "Marvelous MEMS," *IEEE Circuits Devices Mag.*, vol. 22, no. 2, pp. 8–28, Mar./Apr. 2006.

[2] V. Kaajakari, *Practical MEMS*. Las Vegas, NV, USA: Small Gear Pub., 2009.

[3] C. Liu, *Foundations of MEMS*. Englewood Cliffs, NJ, USA: Prentice-Hall, 2011.

[4] N. V. Lavrik, M. J. Sepaniak, and P. G. Datskos, "Cantilever transducers as a platform for chemical and biological sensors," *Rev. Sci. Instrum.*, vol. 75, no. 7, pp. 2229–2253, 2004.

[5] K. M. Hansen and T. Thundat, "Microcantilever biosensors," *Methods*, vol. 37, no. 1, pp. 57–64, 2005.

[6] H.-J. Butt, B. Cappella, and M. Kappl, "Force measurements with the atomic force microscope: Technique, interpretation and applications," *Surf. Sci. Rep.*, vol. 59, nos. 1–6, pp. 1–152, 2005.

[7] A. W. McFarland, M. A. Poggi, L. A. Bottomley, and J. S. Colton, "Characterization of microcantilevers solely by frequency response acquisition," *J. Micromech. Microeng.*, vol. 15, no. 4, pp. 785–791, 2005.

[8] K. C. Neuman and A. Nagy, "Single-molecule force spectroscopy: Optical tweezers, magnetic tweezers and atomic force microscopy," *Nature Methods*, vol. 5, pp. 491–505, May 2008.

[9] S. E. Cross, Y.-S. Jin, J. Rao, and J. K. Gimzewski, "Nanomechanical analysis of cells from cancer patients," *Nature Nanotechnol.*, vol. 2, pp. 780–783, Dec. 2007.

[10] Q. S. Li, G. Y. H. Lee, C. N. Ong, and C. T. Lim, "AFM indentation study of breast cancer cells," *Biochem. Biophys. Res. Commun.*, vol. 374, no. 4, pp. 609–613, 2008.

[11] S. H. Yang, Y. Kim, K. P. Purushotham, J.-M. Yoo, Y.-M. Choi, and N. Dagalakis, "AFM characterization of nanopositioner in-plane stiffnesses," *Sens. Actuators A, Phys.*, vol. 163, no. 1, pp. 383–387, 2010.

[12] J. Rajagopalan and M. T. A. Saif, "MEMS sensors and microsystems for cell mechanobiology," *J. Micromech. Microeng.*, vol. 21, no. 5, p. 054002, 2011.

[13] F. Khoshnoud and C. W. de Silva, "Recent advances in MEMS sensor technology—Biomedical applications," *IEEE Instrum. Meas. Mag.*, vol. 15, no. 1, pp. 8–14, Feb. 2012.

[14] J. E. Sader, I. Larson, P. Mulvaney, and L. R. White, "Method for the calibration of atomic force microscope cantilevers," *Rev. Sci. Instrum.*, vol. 66, no. 7, pp. 3789–3798, Jul. 1995.

[15] J. L. Hutter and J. Bechhoefer, "Calibration of atomic-force microscope tips," *Rev. Sci. Instrum.*, vol. 64, no. 7, pp. 1868–1873, 1993.

[16] R. S. Gates and M. G. Reitsma, "Precise atomic force microscope cantilever spring constant calibration using a reference cantilever array," *Rev. Sci. Instrum.*, vol. 78, no. 8, p. 086101, 2007.

[17] H. J. Pandya, H. T. Kim, R. Roy, and J. P. Desai, "MEMS based low cost piezoresistive microcantilever force sensor and sensor module," *Mater. Sci. Semicond. Process.*, vol. 19, pp. 163–173, Mar. 2014.

[18] S. J. Grutzik, R. S. Gates, Y. B. Gerbig, D. T. Smith, R. F. Cook, and A. T. Zehnder, "Accurate spring constant calibration for very stiff atomic force microscopy cantilevers," *Rev. Sci. Instrum.*, vol. 84, no. 11, pp. 113706-1–113706-8, 2013.

[19] K. Miyamoto, T. Jomori, K. Sugano, O. Tabata, and T. Tsuchiya, "Mechanical calibration of MEMS springs with sub-micro-Newton force resolution," *Sens. Actuators A, Phys.*, vol. 143, no. 1, pp. 136–142, 2008.

[20] S. J. Koch, G. E. Thayer, A. D. Corwin, and M. P. de Boer, "Micromachined piconewton force sensor for biophysics investigations," *Appl. Phys. Lett.*, vol. 89, no. 17, pp. 173901-1–173901-3, 2006.

[21] F. Beyeler *et al.*, "Monolithically fabricated microgripper with integrated force sensor for manipulating microobjects and biological cells aligned in an ultrasonic field," *J. Microelectromech. Syst.*, vol. 16, no. 1, pp. 7–15, Feb. 2007.

[22] K. Kim, X. Liu, Y. Zhang, and Y. Sun, "Nanonewton force-controlled manipulation of biological cells using a monolithic MEMS microgripper with two-axis force feedback," *J. Micromech. Microeng.*, vol. 18, no. 5, p. 055013, 2008.

[23] F. Beyeler, S. Muntwyler, and B. J. Nelson, "A six-axis MEMS force–torque sensor with micro-Newton and nano-Newtonmeter resolution," *J. Microelectromech. Syst.*, vol. 18, no. 2, pp. 433–441, 2009.

[24] J. Rajagopalan, A. Tofangchi, and M. T. A. Saif, "Linear high-resolution BioMEMS force sensors with large measurement range," *J. Microelectromech. Syst.*, vol. 19, no. 6, pp. 1380–1389, Dec. 2010.

[25] K. H.-L. Chau, S. R. Lewis, Y. Zhao, R. T. Howe, S. F. Bart, and R. G. Marcheselli, "An integrated force-balanced capacitive accelerometer for low-*g* applications," *Sens. Actuators A, Phys.*, vol. 54, nos. 1–3, pp. 472–476, 1996.

[26] N. Yazdi, F. Ayazi, and K. Najafi, "Micromachined inertial sensors," *Proc. IEEE*, vol. 86, no. 8, pp. 1640–1659, Aug. 1998.

[27] H. Luo, G. Zhang, L. R. Carley, and G. K. Fedder, "A post-CMOS micromachined lateral accelerometer," *J. Microelectromech. Syst.*, vol. 11, no. 3, pp. 188–195, 2002.

[28] Y. Shen, E. Winder, N. Xi, C. A. Pomeroy, and U. C. Wejinya, "Closed-loop optimal control-enabled piezoelectric microforce sensors," *IEEE/ASME Trans. Mechatronics*, vol. 11, no. 4, pp. 420–427, Aug. 2006.

[29] V. Kempe, *Inertial MEMS: Principles and Practice*. Cambridge, U.K.: Cambridge Univ. Press, 2011.

[30] Y. Liang, L. Xiaowei, C. Weiping, and Z. Zhiping, "High resolution interface circuit for closed-loop accelerometer," *J. Semicond.*, vol. 32, no. 4, p. 045005, 2011.

[31] M. B. Coskun, S. Moore, S. O. R. Moheimani, A. Neild, and T. Alan, "Zero displacement microelectromechanical force sensor using feedback control," *Appl. Phys. Lett.*, vol. 104, no. 15, pp. 153502-1–153502-4, 2014.

[32] A. Mohammadi, A. G. Fowler, Y. K. Yong, and S. O. R. Moheimani, "A feedback controlled MEMS nanopositioner for on-chip high-speed AFM," *J. Microelectromech. Syst.*, vol. 23, no. 3, pp. 610–619, 2013.

[33] B. Krijnen *et al.*, "A single-mask thermal displacement sensor in MEMS," *J. Micromech. Microeng.*, vol. 21, no. 7, p. 074007, 2011.

[34] A. G. Fowler, A. Bazaei, and S. O. R. Moheimani, "Design and analysis of nonuniformly shaped heaters for improved MEMS-based electrothermal displacement sensing," *J. Microelectromech. Syst.*, vol. 22, no. 3, pp. 687–694, 2013.

[35] S. O. R. Moheimani, "Invited review article: Accurate and fast nanopositioning with piezoelectric tube scanners: Emerging trends and future challenges," *Rev. Sci. Instrum.*, vol. 79, no. 7, p. 071101, 2008.

Steven Ian Moore received the Bachelor's degrees in electrical engineering and mathematics from the University of Newcastle, Callaghan, NSW, Australia, in 2012, where he is currently pursuing the Ph.D. degree in electrical engineering with the Laboratory for Dynamics and Control of Nanosystems. His research focus is on the design and implementation of precision motion control and sensing in microelectromechanical systems (MEMS), including applications in MEMS nanopositioners and resonators.

M. Bulut Coskun received the B.Sc. and M.Sc. degrees in mechatronics engineering from Sabanci University, Istanbul, Turkey, in 2009 and 2011, respectively. He is currently pursuing the Ph.D. degree in mechanical engineering with Monash University, Melbourne, VIC, Australia. His research focuses on fabrication and characterization of microelectromechanical force and pressure sensors. He has been involved in the development of flexible and graphene-based sensors.

Tuncay Alan received the Ph.D. degree in theoretical and applied mechanics from Cornell University, Ithaca, NY, USA. Prior to joining Monash University, Melbourne, VIC, Australia, he has been a Researcher with the Delft Institute of Microsystems and Nanoelectronics, Delft, The Netherlands, and the London Centre for Nanotechnology, London, U.K. His research focuses on microelectromechanical systems, microfluidics, and experimental nanomechanics.

Adrian Neild is currently an Australian Research Fellow and Associate Professor with Monash University, Melbourne, VIC, Australia. He received the Ph.D. degree in engineering from the University of Warwick, Coventry, U.K., in 2003. He was a Post-Doctoral Researcher with the Institute for Mechanical Systems, Swiss Federal Institute of Technology Zurich, Zurich, Switzerland. He has been a faculty member with Monash University since 2006, where he cofounded the Laboratory for Microsystems. His research interests are in the fields of microfluidics, microparticle manipulation, microsensors, and other microsystems.

S. O. Reza Moheimani (M'96–SM'00–F'11) received the Doctoral degree from the University of New South Wales in Canberra, Australia, in 1996.

He joined the University of Newcastle in 1997 embarking on a new research program addressing the dynamics and control design issues related to highprecision mechatronic systems. He is the Founder and Director of the Laboratory for Dynamics and Control of Nanosystems, a multimillion-dollar stateof- the-art research facility. He has published over 300 refereed papers and five books and edited volumes. His current research interests include ultra-high-precision mechatronic systems, with particular emphasis on dynamics and control at the nanometer scale, including applications of control and estimation in nanopositioning systems for high-speed scanning probe microscopy, modeling and control of microcantilever-based devices, control of micro-actuators in microelectromechanical systems, and design, modeling and control of micromachined nanopositioners for on-chip atomic force microscopy.

Prof. Moheimani is a fellow of IEEE, IFAC and the Institute of Physics, U.K. His work has been recognized with a number of awards, including the IFAC Nathaniel B. Nichols Medal in 2014, the IFAC Mechatronic Systems Award in 2013, the IEEE Control Systems Technology Award in 2009, the Australian Research Council Future Fellowship in 2009, the IEEE Transactions on Control Systems Technology Outstanding Paper Award in 2007, the Australian Research Council Post Doctoral Fellowship in 1999, and several best student paper awards in various conferences. He has served on the editorial boards of a number of journals, including the IEEE/ASME TRANSACTIONS ON MECHATRONICS, the IEEE TRANSACTIONS ON CONTROL SYSTEMS TECHNOLOGY, and *Control Engineering Practice*. He currently chairs the IFAC Technical Committee on Mechatronic Systems, and has chaired several international conferences and workshops.